The Astrophysical Journal, 871:244 (7pp), 2019 February 1 https://doi.org/10.3847/1538-4357/aafb38

The Period Change of Cyg X-3

Igor I. Antokhin and Anatol M. Cherepashchuk
Moscow Lomonosov State University, Sternberg State Astronomical Institute, 119992 Universitetsky prospect, 13, Moscow, Russia; igor@sai.msu.ru
Received 2018 July 2; revised 2018 December 26; accepted 2018 December 27; published 2019 February 5

Abstract

By using available archival X-ray data, we significantly extended the list of times of X-ray minima. The new list includes 65 data points obtained by critically reanalyzing *RXTE* ASM data, 88 data points based on observations by *MAXI*, and 2 data points based on observations by *SUZAKU* and *AstroSat*. Analyzing the data along with times of X-ray minima available from the literature, we provide the most accurate estimate of the rate of period change to date. We do not confirm the existence of a second derivative of the orbital period suggested by some authors earlier. Instead, we find that the changes in the period can be fit by a sum of quadratic and sinusoidal functions. The period of sinusoidal variations is 15.79 yr. They can be related either to apsidal motion in the close binary with eccentricity $e \simeq 0.03$ or to the presence of a third body with a mass of about 0.7 $M_{\odot}$ located at a distance ~16 au from the close binary.

Key words: accretion, accretion disks – binaries: close – stars: individual (Cyg X-3) – X-rays: binaries

Supporting material: machine-readable table

1. Introduction

Cyg X-3 is a rare X-ray binary system consisting of a WN4-8 star and a compact object (van Kerkwijk et al. 1992, 1996). The only two other (much less studied) binaries of this type are IC10 X-1 (WNE+C, $p = 1\overset{d}{.}5$, Prestwich et al. 2007; Silverman & Fillipenko 2008) and NGC300 X-1 (WN5+C, $p = 1\overset{d}{.}3$, Crowther et al. 2010). The orbital period of Cyg X-3 is about 4.8 hr. Little is known about the system inclination and mass functions. Hanson et al. (2000) discovered a detail regarding absorption in the IR spectrum, indicating that radial velocity may reflect orbital motion of the WR component. Vilhu et al. (2009) found Doppler shifts of some X-ray emission lines that may reflect orbital motion of the compact object. Critically analyzing these data, Zdziarski et al. (2013) estimated the mass ratio in the system $M_C/M_{WR} = 0.23^{+0.09}_{-0.06}$. Then, using a relation between the binary period derivative and the mass-loss rate of the WR component and the relationship between the mass-loss rate and the mass for WR stars of the WN type, they were able to estimate the mass of the WR component, and, subsequently, the mass of the compact object. The latter turned out to be $M_C = 2.4^{+2.1}_{-1.1} M_{\odot}$. Recently, Koljonen & Maccarone (2017) showed that the IR lines found by Hanson et al. (2000) most likely do not reflect the motion of the WR component and instead originated in the WR wind. Thus, the conclusion of Zdziarski et al. (2013) is refuted and the origin of the compact object remains unclear—it could be either a neutron star (NS) or a black hole (BH). For more information regarding the physical properties of the system, see also Zdziarski et al. (2018).

The change of the binary period has been studied by many authors since 1975 (see Bhargava et al. 2017 and references therein; the full list of previous papers on the subject is also provided in the references to Table 1). These authors used data obtained with various X-ray satellites. The data for most satellites cover only a limited number of orbital cycles. Furthermore, there is strong irregular variability of the source along with its orbital variations. *RXTE* ASM and *MAXI* missions, on the other hand, have the big advantage of providing continuous monitoring of Cyg X-3 on a time span of 22 yr. We take this opportunity to refine our knowledge about the period evolution. In Section 2 we describe the archival data analyzed in this paper. In Section 3 the method for finding the times of X-ray minima and their errors is explained. Section 4 presents the results of fitting these data by various models of period change. In Section 5 we discuss a possible nature of the discovered sinusoidal variations of the period. Irregular and abrupt changes in the $(O - C)$ residuals are discussed in Section 6. Section 7 contains a summary of our results.

2. Archival Data

2.1. RXTE *ASM*

The ASM on board the *RXTE* satellite (Levine et al. 1996) had three scanning cameras with large fields of view (FOVs, $6° \times 90°$ for each camera). A single exposure was 90 s, then the telescope moved to another position. The light curve in the total energy range 1.3–12 keV was downloaded from the *RXTE* Guest Observer Facility provided by HEASARC. The total number of data points was 97,996, covering the period from 1996 January to 2011 December. Among these, 1062 data points had negative fluxes, probably due to marginal detection when the source was very weak. We excluded strongly negative fluxes (such that cts $+ 1\sigma_{cts} < 0$) from further analysis due to their unreliability (266 data points) and kept the others (796 data points, such that cts $+ 1\sigma_{cts} \geqslant 0$).

2.2. SUZAKU

Cyg X-3 was observed by *SUZAKU* in 2006 November for about 50 hr. The data useful for extracting the light curve were obtained with three XIS (X-ray Imaging Spectrometers) instruments (XI0, XI1, and XI3). The full FOV is $18' \times 18'$. The source, however, was observed in a burst mode with the window size $4\overset{'}{.}5 \times 18'$. The energy range covered by XIS is 0.2–12 keV. We downloaded the event lists and auxiliary files from the HEASARC archive facility. The data were processed with the *Ftools* package. To increase the signal-to-noise ratio, we combined the light curves (in the total energy range) from XI0 and XI3 (XI1 cannot be combined with other XIS

Table 1
Times of X-Ray Minima and Orbit Numbers

Time of X-Ray Minimum T_n (MJD)	Error in T_n (days)	Number of Orbital Cycle n	Reference
40949.4201[a]	0.0162	0	1
40987.1629	0.0037	189	1
40987.9555	0.0064	193	1
40991.1625	0.0092	209	1
41022.4995[a]	0.0140	366	1

Note.
[a] The original paper contained a typographic error in this number, which was corrected by Elsner et al. (1980).
References. (1) Leach et al. (1975); (2) Mason & Sanford (1979); (3) Parsignault et al. (1976); (4) Manzo et al. (1978); (5) Lamb et al. (1979); (6) Elsner et al. (1980); (7) van der Klis & Bonnet-Bidaut (1981); (8) van der Klis & Bonnet-Bidaut (1989); (9) Kitamoto et al. (1987); (10) Kitamoto et al. (1992); (11) Kitamoto et al. (1995); (12) Singh et al. (2002); (13) Current study.

(This table is available in its entirety in machine-readable form.)

instruments as its CCD has a distinctly different response). The light curve contains 621 measurements.

2.3. *MAXI* SCAN Data

The *MAXI* on board the International Space Station (ISS) is a scanning X-ray telescope launched in 2009 (Matsuoka et al. 2009). The fields of view of its two instruments, GSC and SSC ($1\overset{\circ}{.}5 \times 160^\circ$ and $1\overset{\circ}{.}5 \times 90^\circ$ respectively), are oriented perpendicularly to ISS orbit and thus allow us to observe many objects at once nearly every ISS orbit (about 90 minutes), subject to ISS orbit precession. An object located along a great circle stays in the FOV for 45 s; slanted objects stay longer. The *MAXI* website provides links to light curves averaged over various time intervals, but also a link to the so-called SCAN data, which represent individual observations obtained within one ISS orbit. We downloaded GSC SCAN data for Cyg X-3 from the *MAXI* website. The data cover the period from 2009 August 15 to 2018 March 24, with 25,042 measurements in total. Among them, about 23,000 have exposure times from 47 to 53 s, the rest of measurements have exposures from about 20 to 190 s. For each measurement, the data consist of fluxes in 2–20, 2–4, 4–10, and 10–20 keV bands. To study the period change and long-term variability, we used the data for the total band 2–20 keV.

2.4. AstroSat

Cyg X-3 was observed by *AstroSat* for 1.5 days in 2015 November. The useful data were obtained by the SXT instrument, the energy range is 0.3–8 keV. We downloaded the light curve using a link provided in Bhargava et al. (2017). The number of measurements is 192.

The times of observations for all archival data were corrected to the solar system barycenter.

2.5. Data Segments

The data from *SUZAKU* and *AstroSat* cover short time intervals and thus provide only one time of X-ray minimum each. To determine X-ray minima times for *RXTE* ASM and *MAXI* data, the corresponding data sets were divided by segments as follows:

1. The average length of a segment should be relatively small (tens of days).
2. The object should be either in the high or low state within a segment, without transitions between the two.
3. A segment should not include strong flares significantly affecting the shape of the light curve.

These rules, being applied, resulted in one data segment for *SUZAKU* and *AstroSat* (each), 65 data segments for *RXTE* ASM, and 88 data segments for *MAXI*. *RXTE* ASM data are rather sparse so the length of a segment varied from about 50 to 90 days. For *MAXI*, these were from about 15 to 30 days.

3. The Method to Determine a Time of X-Ray Minimum and Its Error

A data segment includes many orbital cycles. The time of X-ray minimum for a data segment is usually found by fitting a model light curve to the observed one within a segment. The time of the model light curve zero phase, which is closest to the middle time of the segment is then taken as the time of minimum for that segment. Early authors fitted the observed light curve by a sine function. However, since the work of van der Klis & Bonnet-Bidaut (1989) it has been common to fit the observed light curve by the template light curve suggested in this paper. The phase of the template is adjusted so as to coincide with the sinusoidal minimum phase, to avoid systematic shifts. In the most general case, such fitting has four parameters: the scaling factor for the amplitude of the template, its mean flux, the local period, and the time of X-ray minimum for a data segment. Most previous authors searched for all of these parameters.

Note that the authors of the two latest papers on the subject (Singh et al. 2002; Bhargava et al. 2017) used a fixed value of a local period. Singh et al. (2002) used a constant period for all data segments they analyzed. Bhargava et al. (2017) used two methods—a constant period and a local period computed from a previously found rate of period change. In both cases the value of the local period was fixed while searching for the time of X-ray minimum. These methods are subject to systematic error in the value of the time of minimum and to underestimation of its uncertainty. Indeed, when searching for a period and time of minimum of a periodic function, the values found by fitting a model may be correlated. One should instead use the full covariance information provided by an optimizer to get correct estimates of the parameter values and their confidence intervals.

Intrinsic variations of the light curve in most cases make the value of χ^2 larger than the number of d.o.f.. In our study, a typical reduced χ^2_ν was about 3, as in most of previous studies. Thus, formal error estimates of the minima times are unreliable. To avoid this problem, many previous authors artificially increased data errors such that the reduced χ^2_ν became equal to unity and then estimated the 1σ uncertainty of the time of minimum from the $\Delta\chi^2 = 1$ principle. However, this method is statistically incorrect. It can be used only if one is certain that deviations of the data from the model have purely Gaussian probability distribution, which is definitely not the case for Cyg X-3. This is why even after artificially increasing data errors, the error of a time of minimum obtained with the $\Delta\chi^2 = 1$ method, is underestimated. To get a more reasonable

value of the error, some authors quadratically added a fixed error (e.g., 0.002, Kitamoto et al. 1995), to compensate for the systematic component in the deviations of the data from the model. The validity of such an approach is doubtful.

Also note that Singh et al. (2002) and Bhargava et al. (2017) used another method to estimate the errors of the times of minima. They searched for its best value by cross-correlating the template light curve with the data and then by fitting the peak of the cross-correlation function by a Gaussian or parabola. The position of the Gaussian/parabola maximum was taken as the time of minimum, and the error of this position (that is the error of the approximation) as the error of the time of minimum. This procedure of estimating the errors may not always be appropriate. The error of the peak position is defined by the quality of the data and not by the error of the parametric approximation of the peak. The former can be used solely if one proves that the error of the peak position is much smaller than the error of its parametric approximation. This is what was assumed by Bhargava et al. (2017), without explicitly demonstrating that this was indeed the case. Moving ahead, we can say that our error estimates for the same data as those used by Bhargava et al. (2017), are about two times larger than theirs.

Concluding, we can say that searching for a time of minimum by using a fixed value of the local period may lead to systematic errors in its value. Using the $\Delta\chi^2 = 1$ method underestimates the error of this value, due to systematic deviations of the data from the template light curve. Using the error of a parametric approximation of the cross-correlation function as the error of the time of minimum may not always be appropriate. For this reason, in the current work we not only added the *MAXI* and *SUZAKU* data to the whole data set, but also reanalyzed the *RXTE* ASM and *AstroSat* data. All four parameters mentioned above, were searched for when fitting observed light curves by the template. The Nelder–Mead method was used as the minimization routine.

To estimate the error of a time of minimum, we used a variant of Monte Carlo simulations known as the *Bootstrapping* method (Davison & Hinkley 1997), in its *resampling residuals* version. The method goes as follows. Let us designate the data points to fit as x_i, y_i, ($i = 1, \ldots, n$), where x_i is the independent variable.

1. Fit the model, compute the fitted values y_i^f, and retain residuals $r_i = y_i - y_i^f$.
2. Create a new synthetic data set by adding a randomly resampled residual to y_i^f: $y_i^s = y_i^f + r_j$, where j is selected randomly from the list (1, ..., n) for every i.
3. Refit the model using the just created synthetic data set y_i^s and retain the obtained values of the parameters (in our case the time of minimum and period).
4. Repeat steps 2 and 3 a large number of times N.

After the simulations are finished, the obtained N values of every parameter can be used to construct its empirical probability distribution and to estimate various distribution parameters such as standard deviation of a parameter etc. The advantage of this method over $\Delta\chi^2 = 1$ is that it does not require the deviations of the data from the model to be Gaussian. The only requirement is that the probability distribution of residuals does not vary much in the vicinity of the parameter's true value (i.e., the probability distribution of the residuals with our best-fit template is about the same as it would be if the template were computed with the (unknown) true values of the time of minimum and period). Of course, such an uncertainty estimate is still based on the assumption that the model is accepted.

Our numerical experiments have shown that 2000 simulations were sufficient to get reasonable estimates of σ for a time of minimum and period. Further increasing the number of simulations did not change the obtained values. In Figure 1 an example of simulations for one *MAXI* data segment is shown. In most cases, the shape of the empirical probability functions is nearly Gaussian, with typical excess kurtosis values from 0 to $\sim$0.5.

Note that an alternative to *resampling residuals* is the so-called *case resampling*. Instead of steps 1 and 2 above, a new synthetic data set is created by randomly choosing data points themselves, with replacement. The method is more suitable for cases when both independent and response variables are random. If the independent variable is set by the researcher or is known with high accuracy (such as time in our case), *case resampling* causes loss of information in any given synthetic sample. Another downside of *case resampling* is its sensitivity to the specific distribution of data points and phases that constrain the fit parameters. On the other hand, in practice, if the number of data points is large and the independent variable is more or less uniformly distributed within its range (in our case phase interval 0–1), then the results given by *case resampling* should be similar to those given by *resampling residuals*. To test our results, we also processed all data segments using *case resampling*. For the majority of the data segments, the uncertainties obtained with the two methods differ by 1–2%. However, when *case resampling* was used, in several cases the empirical probability distributions were extremely different from Gaussian (e.g., two-peaked), apparently due to specific flux/phase distribution. Residual resampling provided more consistent results in these cases. Given these considerations, we adopted the uncertainties obtained with the *resampling residuals* method.

Table 1 lists all data on times of minima and orbit numbers (in increasing order) gathered from the literature (115 values) and obtained in the current study (155). The table does not include the local periods as their errors are usually quite large (see Figure 1), making them not too useful.

4. The Period Change

In Table 2 the results of various fits to the times of X-ray minima are shown. Fits with some of the models are shown in Figure 2. As in the previous studies, we started with linear, quadratic, and cubic models. Several previous authors (e.g., Kitamoto et al. 1995) argued that the cubic model provided a better fit than the quadratic one. Our results clearly show that this is not the case (see Table 2 and Figure 2(b)). It is immediately evident that residuals of the quadratic model have sinusoidal shape, except for 12 data points in the beginning of the whole observation interval. These 12 data points show strong deviations in all models, which was also the case in all previous studies. The times of minima are from Leach et al. (1975), one of the first papers on the subject. The authors obtained them by fitting a sine function to *Uhuru* X-ray light curves. As these data points clearly show large systematic deviations from any model, we repeated the quadratic fit excluding these data. χ^2 values for the linear, quadratic, and cubic models are significantly higher than the number of d.o.f.,

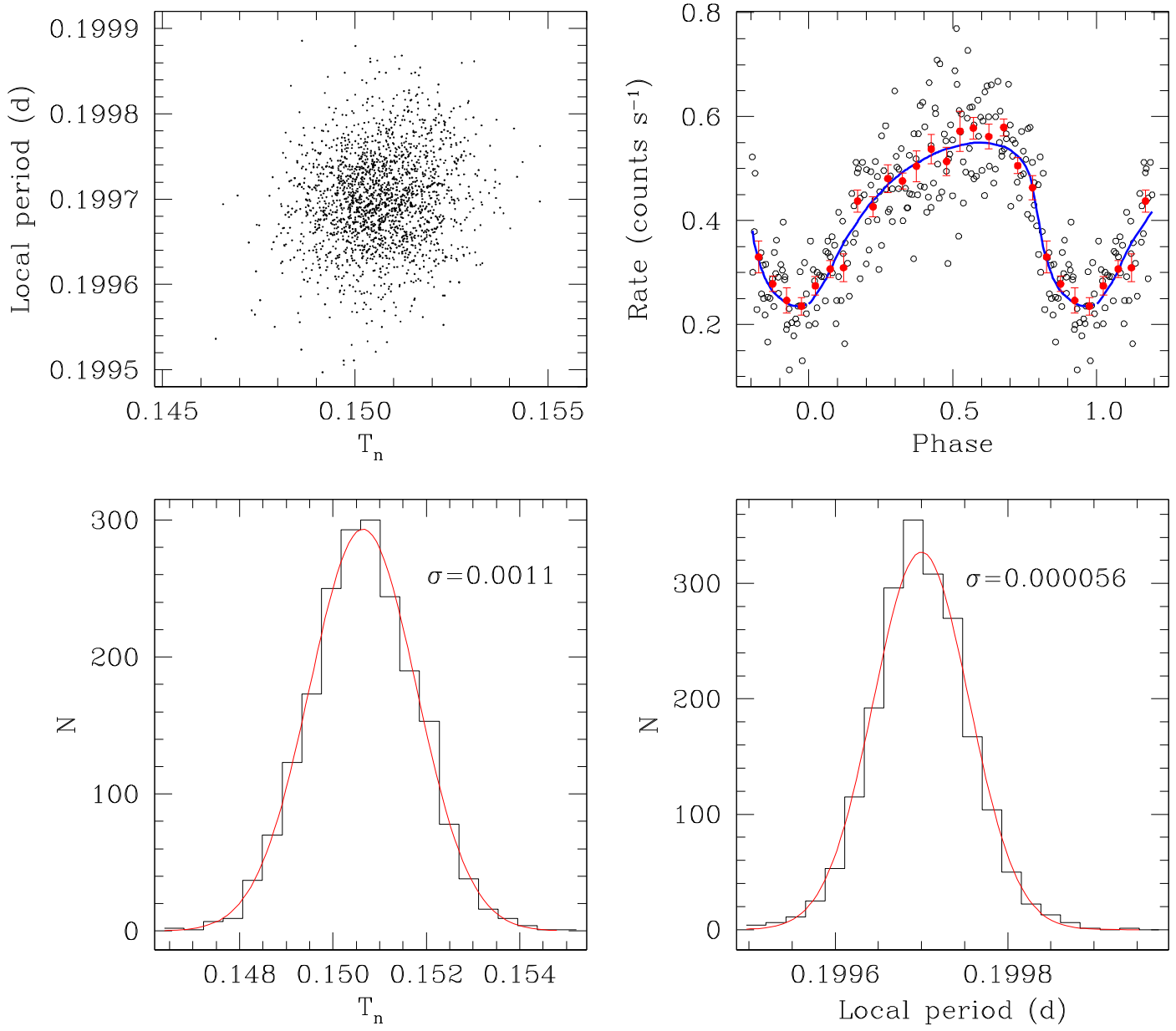

Figure 1. Example of the *Bootstrapping residuals* method for a *MAXI* data segment. Top left: distribution of the time of minimum T_n and period, each of 2000 dots is the result of a single fit of a synthetic data set. The integer part of T_n is omitted to avoid clutter. Top right: the best-fit template light curve (solid blue line), the observed data (open dots, the errors of the individual data points are not shown to avoid clutter), and the mean observed light curve (red solid dots). Bottom left: the empirical probability function for the time of minimum (the histogram). Bottom right: same for the local period. Red lines in bottom plots show Gaussian functions with the mean and σ values of the time of X-ray minimum and period computed from 2000 Monte Carlo simulations.

so the formal errors of their parameters presented in Table 2 should be taken with caution.

To fit the sinusoidal variations seen in the residuals of the quadratic model, we used a model consisting of a sum of quadratic and sinusoidal terms:

$$T_n = T_0 + P_0 n + cn^2 + a_s \sin\left(\frac{2\pi}{P_s}(n - n_{0s})\right),$$

where $c = P_0\dot{P}/2$, a_s is the amplitude of the sine function, P_s is the sine period, n_{0s} is the zero epoch of sinusoidal variations (in orbital cycles). The fit (omitting the Leach et al. 1975 data) is shown in Figure 2(c), and the model parameters are listed in Table 2. The χ^2 value of the fit is much smaller than that for the quadratic model, but still too large to formally accept the model. As the remaining deviations of the data from the model look more or less random, to estimate errors of the parameters in this case, we used the same *Bootstrapping residuals* method which was used when fitting the template light curve to X-ray data. We did not use the method for the other models as the corresponding residuals are clearly not random.

At least part of the remaining deviations in Figure 2(d) consist of irregular and abrupt changes of the residuals. We will discuss them below.

5. The Nature of the Sinusoidal Component in the Period Change

Theoretically speaking, the sinusoidal variations of the orbital period could be explained by three mechanisms:

Table 2
Ephemeris of Different Models

1. Linear ephemeris: $T_n = T_0 + Pn$
$\chi^2 = 120737$ for 268 d.o.f
$T_0 = 40949.31479 \pm 0.00021$ MJD
$P = 0.1996895309 \pm 0.0000000037$ days
2. Quadratic ephemeris: $T_n = T_0 + P_0 n + cn^2$
$\chi^2 = 931.3$ for 267 d.o.f
$T_0 = 40949.39010 \pm 0.00031$ MJD
$P_0 = 0.19968459 \pm 0.000000015$ days
$c = (5.60 \pm 0.02) \times 10^{-11}$ days
$\dot{P} = (5.61 \pm 0.02) \times 10^{-10}$
3. Cubic ephemeris: $T_n = T_0 + P_0 n + cn^2 + dn^3$
$\chi^2 = 931.1$ for 266 d.o.f
$T_0 = 40949.39028 \pm 0.00054$ MJD
$P_0 = 0.19968458 \pm 0.000000056$ days
$c = (5.66 \pm 0.14) \times 10^{-11}$ days
$d = (-3.98 \pm 9.8) \times 10^{-18}$ days
$\dot{P} = (5.67 \pm 0.14) \times 10^{-10}$
4. Quadratic ephemeris without Leach et al. (1975) data:
$\chi^2 = 768.3$ for 267 d.o.f
$T_0 = 40949.38955 \pm 0.00031$ MJD
$P_0 = 0.19968462 \pm 0.000000015$ days
$c = (5.58 \pm 0.02) \times 10^{-11}$ days
$\dot{P} = (5.59 \pm 0.02) \times 10^{-10}$
5. Quadratic + sinusoidal ephemeris
without Leach et al. (1975) data:
$T_n = T_0 + P_0 n + cn^2 + a_s \sin(2\pi/P_s(n - n_{0s}))$
$\chi^2 = 491.9$ for 252 d.o.f
$T_0 = 40949.39077 \pm 0.00002$ MJD
$P_0 = 0.19968457 \pm 0.000000002$ days
$c = (5.620 \pm 0.002) \times 10^{-11}$ days
$\dot{P} = (5.629 \pm 0.002) \times 10^{-10}$
$a_s = 0.00205 \pm 0.00001$ days
$P_s = 28888 \pm 40$ orbital cycles (15.79 ± 0.02 yr)
$n_{0s} = 50621 \pm 29$

1. Regular changes in the mass-loss rate of the WR star.
2. Apsidal motion in the system.
3. A presence of a third body.

The first hypothesis is ruled out by simple numerical estimates. Although the wind of the WR star is probably not spherically symmetric, we can roughly relate $\dot{P}$ to $\dot{M}$ by using a relationship for a spherical case: $2\dot{M}/M = \dot{P}/P$, where M is the total mass of a binary and P is the orbital period. Let us assume that $\dot{M}(n) = \dot{M}_0 + a_{\dot{M}} \sin(2\pi/P_s(n - n_{0s}))$. After some simple algebra, the expected amplitude of the (sinusoidal) residuals with the quadratic ephemeris

$$a_s[\text{days}] = \frac{P_0[\text{days}]P_s[\text{yr}]}{\pi M[M_\odot]} a_{\dot{M}}[M_\odot\ \text{yr}^{-1}].$$

Substituting the values from Table 2 and $M = 15\ M_\odot$, we obtain $a_{\dot{M}} \simeq 0.03\ M_\odot\ \text{yr}^{-1}$. This means that to explain the observed sinusoidal variations of the orbital period, the WR star has to *change* its mass-loss rate by $0.03\ M_\odot\ \text{yr}^{-1}$ which is many orders of magnitude beyond the whole mass-loss rate of the WR star ($\sim 10^{-5}\ M_\odot$). More precise estimates taking into account, e.g., accretion onto the compact object can be done following Tout & Hall (1991), but they would give similar results. The accretion occurs through the WR wind, either by direct capture or through the focused wind (Koljonen & Maccarone 2017). In the first case, only a tiny fraction ($\lesssim 0.01$) of the angular momentum of the donor (WR star) is accreted by the compact object. In the second case, the extreme value of the fraction may reach 0.2 (Koljonen & Maccarone 2017). Thus, the change in the above simple estimate may be about 20% at most. Above all, this hypothesis assumes an underlying mechanism that forces strictly periodic long-term changes of the WR mass-loss rate. Such mechanisms are currently unknown.

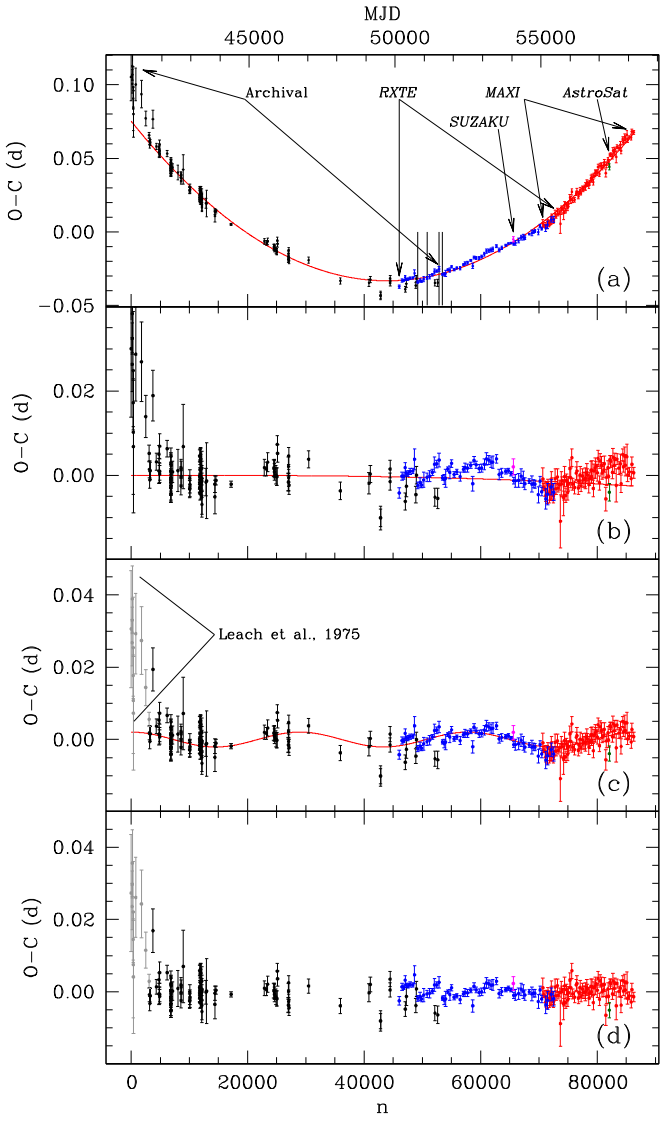

Figure 2. Various fits to the times of X-ray minima of Cyg X-3. Archival data are shown by black dots, *RXTE* ASM data by blue dots, *MAXI* data by red dots, *SUZAKU* and *AstroSat* data points by magenta and green dots respectively. (a) Residuals of model 1. The solid red line shows the quadratic term of model 2. The arrows show the time intervals covered by archival data and various X-ray missions. (b) Residuals of the quadratic part of model 3. The red solid line is the cubic term of the model. (c) Residuals of the quadratic part of model 5. The red solid line is the sinusoidal term of the model. (d) Residuals of model 5. Leach et al. (1975) data not used in the fits are shown in light gray.

With the data available, the second hypothesis can be verified in three ways. First, Batten (1973, on page 88) gives a formula for the amplitude of period variations caused by apsidal motion: $a_s \simeq eP_s/\pi$. Using our values for a_s and P_s, we obtain a reasonable value $e \simeq 0.033$. Second, on page 124, he gives a formula (2) for the ratio of the orbital and apsidal periods. While the input parameters of this formula—the mass

ratio, the apsidal parameter, and the radius of the WR star—are not known precisely, using reasonable estimates for the former and two limiting values of the WR helium core radius 1 and $2\,R_\odot$, we obtain the range of the possible apsidal period, 140 days–12 yr. This is not surprising given that the system is extremely close. Third, the distance between the orbital phases of the two eclipses in a binary with apsidal motion change over time. From celestial mechanics, the maximal change is $2e(1 + \mathrm{cosec}^2 i)/\pi$. Substituting e found just above and $i = 43°$ (Zdziarski et al. 2013), the value obtained is ∼0.07. While there is no secondary minimum in the X-ray light curve of Cyg X-3, the above value gives a characteristic phase scale for the alleged variations in the light curve. The obtained value is rather small and such variations, if present, could easily be unnoticed. We conclude that the apsidal motion hypothesis cannot be ruled out by the available data.

Let us now estimate the parameters of the third-body configuration. The distance from the close binary to the center of mass of the alleged triple system is determined by the light equation $a_1 \sin i = ca_s$, which results in $a_1 = 1.08 \times 10^{13}$ cm (about 0.72 au). Making simplifying assumptions that (i) the third body and the close binary orbits lie in the same plane, (ii) the orbit of the third body is circular, and (iii) the mass of the close binary (WR+C) is 15 $M_\odot$, from the third *Kepler*'s law we obtain $M_3 \simeq 0.7\,M_\odot$, the distance of the third body from the center of mass of the triple system is $a_2 \simeq 16$ au. The ratio of a_2 to the orbital size of the close binary $\sim 3.5\,R_\odot$ is large and representative of a hierarchical triple system.

6. Irregular Changes of the Residuals

The residuals in Figure 2(a) show several abrupt changes in the interval of MJD 50,000–54,000. The zoomed part of the plot is shown in Figure 3, upper plot. Note that these changes were also present in Singh et al. (2002), although they were not as evident as in our study, due to the smaller amount of *RXTE* ASM data used by the authors.

Possible physical explanations must be necessarily related to changes of the angular momentum, e.g., through the change of the WR mass-loss rate. Note that the decrease of the mass-loss rate cannot decrease the period, which will still increase just at a lower pace. Such a change could lead to the apparent decrease of the period only if the estimated period just before a drop is overestimated. However, simple analysis shows that, to obtain the observed effect, even if the WR mass-loss rate drops to zero, the period before the drop has to be overestimated by about 10^{-6} days. This is about three orders of magnitude larger than the uncertainty of the period obtained in our study and thus highly unlikely. One could also speculate that the drop might be caused by a blob leaving the system in one of the jets, producing an angular momentum "kick." As the jet speed is about half of the speed of light (Marti et al. 2001), the blob mass need not to be too high. Still, simple estimates based on jet orientation (Zdziarski et al. 2018) show that to explain the observed effect, the mass of such a blob should be equal to approximately $10^{-7}\,M_\odot$. The mass-loss rate of the WR star is about $10^{-5}\,M_\odot$ yr^{-1}, and the accretion rate is probably $\leqslant 0.01$ of this value. Thus, it seems practically impossible that such a blob would have the mass accreted by the compact object during a year.

The actual explanation of the changes comes from close inspection of the light curves in the data segments in question.

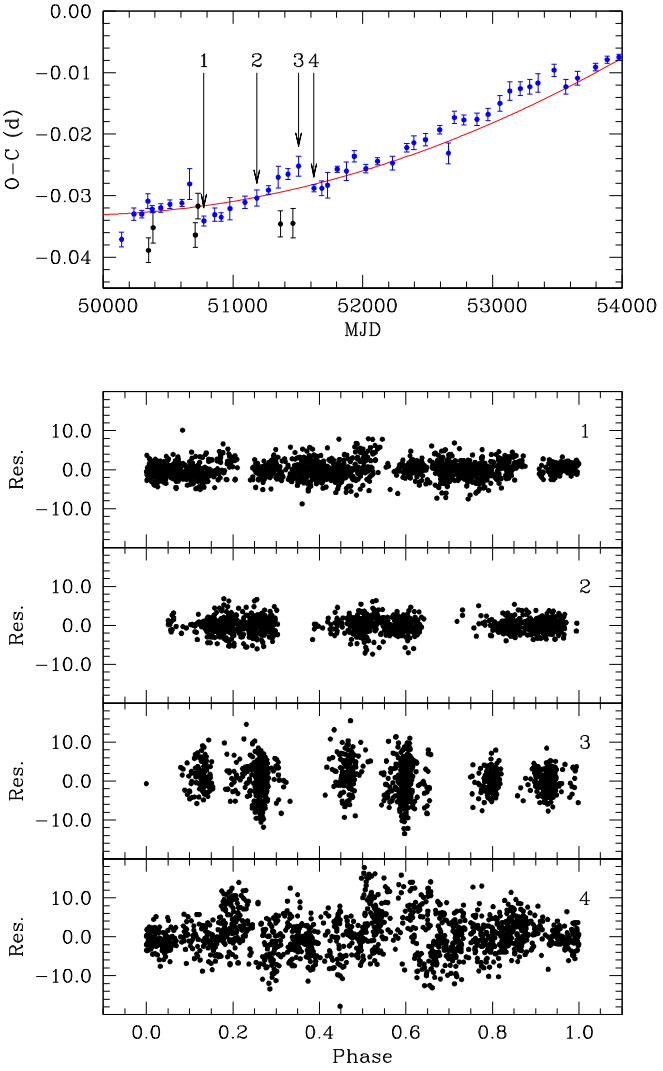

Figure 3. Irregular changes of the residuals from Figure 2(a) and the orbital phase coverage for selected *RXTE* ASM data. Upper plot: a zoomed part of Figure 2(a) showing the changes. Bottom plots: residuals of the best-fit light-curve models for four characteristic data segments 1–4 (shown by arrows in the upper plot).

The residuals of the best-fit light-curve model for four characteristic data segments are shown in the bottom plots in Figure 3. Note that the phase coverage for the data segment 4 (immediately after a drop) is nearly uniform. On the other hand, the light curve for the data segment 3 (immediately before the drop) has several gaps in the orbital phase. Inspection of the previous data segments in the time interval ∼50,800–51,500 (one "tooth" of the observed jigsaw pattern) shows that the phase gaps are progressively increasing with time (residual curves 1–3). As a consequence, the corresponding model fits do not use the missing parts of the observed light curves, causing slight progressively increasing systematic shifts in the best-fit parameters, including the times of X-ray minima. Thus, the observed jigsaw pattern is related to the temporal distribution of *RXTE* ASM data in the MJD 50,000–54,000 interval.

To check how these systematic changes could influence the parameters of the period change models listed in Table 2, we repeated the fits with these models excluding all *RXTE* ASM data segments with gaps in the light curves from the list of the

times of X-ray minima. The resulting best-fit parameters for all models were within the uncertainties listed in Table 2.

7. Conclusions

The available literature on the period change of Cyg X-3 provides 115 times of X-ray minima. By using archival observations of *RXTE* ASM, *MAXI*, *SUZAKU*, and *AstroSat*, we added 155 new times of minima to the list. Our analysis of these data yields the most accurate estimate of the rate of period change to date.

We do not confirm the existence of a second derivative of the orbital period previously suggested by some authors. Instead, we find that the changes in the period can be fit by a sum of quadratic and sinusoidal functions. The period of sinusoidal variations is 15.79 yr. They can be related either to apsidal motion in the close binary with eccentricity $e \simeq 0.03$ or to a presence of a third body with the mass of about 0.7 $M_{\odot}$ located at a distance of $\sim$16 au from the close binary.

The jigsaw pattern in the residuals between the best-fit ephemeris and the data in the MJD 50,000–54,000 interval is caused by the temporal distribution of *RXTE* ASM data within that interval. The influence of the systematic effects in the residuals on the parameters of the period change is negligible.

We thank Prof. K.A. Postnov for valuable discussions and the referee for valuable suggestions. This research has made use of *RXTE* ASM and *SUZAKU* data obtained through the High Energy Astrophysics Science Archive Research Center Online Service, provided by the NASA/Goddard Space Flight Center, and also of the data from the *AstroSat* mission of the Indian Space Research Organization (ISRO), archived at the Indian Space Science Data Centre (ISSDC). This research has also made use of the *MAXI* data provided by RIKEN, JAXA, and the *MAXI* team. Authors acknowledge support by the Russian Science Foundation grant 17-12-01241.

ORCID iDs

Igor I. Antokhin https://orcid.org/0000-0002-3561-8148
Anatol M. Cherepashchuk https://orcid.org/0000-0001-5595-2285

References

Batten, A. H. 1973, Binary and Multiple Systems of Stars (Oxford: Pergamon)
Bhargava, Y., Rao, A. R., Singh, K. P., et al. 2017, ApJ, 849, 141
Crowther, P. A., Barnard, R., & Carpano, S. 2010, MNRAS, 403, L41
Davison, A. C., & Hinkley, D. V. 1997, Bootstrap Methods and their Application (Cambridge: Cambridge Univ. Press)
Elsner, R. F., Ghosh, P., & Darbro, W. 1980, ApJ, 239, 335
Hanson, M. M., Still, M. D., & Fender, R. P. 2000, ApJ, 541, 308
Kitamoto, S., Hirano, A., Kawashima, K., et al. 1995, PASJ, 47, 233
Kitamoto, S., Miyamoto, S., Matsui, W., & Inoue, H. 1987, PASJ, 39, 259
Kitamoto, S., Mizobuchi, S., Yamashita, K., et al. 1992, ApJ, 384, 263
Koljonen, K. I. I., & Maccarone, T. J. 2017, MNRAS, 472, 2181
Lamb, R. C., Dower, R. G., & Fickle, R. K. 1979, ApJL, 229, L19
Leach, R. W., Murray, S. S., Schreier, E. J., et al. 1975, ApJ, 199, 184
Levine, A. M., Bradt, H., Cui, W., et al. 1996, ApJL, 469, L33
Manzo, G., Molteni, D., & Robba, N. R. 1978, A&A, 70, 317
Marti, J., Paredes, J. M., & Peracaula, M. 2001, A&A, 375, 476
Mason, K. O., & Sanford, P. W. 1979, MNRAS, 189, 9
Matsuoka, M., Kawasaki, K., & Ueno, S. 2009, PASJ, 61, 999
Parsignault, D. R., Schreier, E., Grindlay, J., & Gursky, H. 1976, ApJL, 209, L73
Prestwich, A. H., Kilgard, R., Crowther, P. A., et al. 2007, ApJL, 669, L21
Silverman, J. M., & Fillipenko, A. V. 2008, ApJL, 678, L17
Singh, N. S., Naik, S., Paul, B., et al. 2002, A&A, 392, 161
Tout, C. A., & Hall, D. S. 1991, MNRAS, 253, 9
van der Klis, M., & Bonnet-Bidaut, J. M. 1981, A&A, 95, L5
van der Klis, M., & Bonnet-Bidaut, J. M. 1989, A&A, 214, 203
van Kerkwijk, M. H., Charles, P. A., Geballe, T. R., et al. 1992, Natur, 355, 703
van Kerkwijk, M. H., Geballe, T. R., King, D. L., et al. 1996, A&A, 314, 521
Vilhu, O., Hakala, P., Hannikainen, D. C., McCollough, M., & Koljonen, K. 2009, A&A, 501, 679
Zdziarski, A. A., Malyshev, D., Dubus, G., et al. 2018, MNRAS, 479, 4399
Zdziarski, A. A., Mikołajewska, J., & Belczyński, K. 2013, MNRAS, 429, L104